Archaeological Prospection
Archaeol. Prospect. **9999**, (2016)
Published online in Wiley Online Library
(wileyonlinelibrary.com) DOI: 10.1002/arp.1541

The Use of Geophysical Prospections to Map Ancient Hydraulic Works: The Triglio Underground Aqueduct (Apulia, Southern Italy)

GIOVANNI LEUCCI[1]*, MARIO PARISE[2], MARIANGELA SAMMARCO[3] AND GIUSEPPE SCARDOZZI[1]

[1] *CNR-IBAM, National Research Council of Italy, Institute for Archaeological and Monumental Heritage, Strada per Monteroni, Campus Universitario, Lecce, Italy*
[2] *CNR-IRPI, National Research Council of Italy, Institute of Research for the Hydrogeological Protection, Via Amendola 122 I, Bari, Italy*
[3] *Department of Cultural Heritage, University of Salento, Via D. Birago 64, Lecce, Italy*

ABSTRACT This paper presents an integrated analysis using ground-penetrating radar (GPR) and electrical resistivity tomography (ERT) studies to map the Triglio underground aqueduct that in Roman times supplied fresh water to the ancient town of *Tarentum*, modern Taranto, Apulia region, Italy. The study area includes an expansion project of a nearby limestone quarry where mining activity is related to the production of a steel factory (ILVA). The aim was to develop methods for detection and mapping of the geometry of the underground aqueduct. Seven GPR reflection profiles were acquired across and parallel to the hypothesized extent of the aqueduct, while the ERT method was used to understand the stratigraphy of the area and tie reflections to geological units.
Well-preserved vertical shafts for ventilation and inspection of the ancient underground hydraulic work were investigated and used as models for GPR exploration. The GPR profiles, interpreted using both the trace amplitude analysis and the forward modelling, showed reflection features from the main horizontal tunnel of the ancient aqueduct. The void space within the aqueduct, usually the ceiling–air interface, was discovered and mapped using reflections profiles both parallel to the linear feature, but also crossing it, and differentiated from similar looking geological features. Copyright © 2016 John Wiley & Sons, Ltd.

Key words: Hydraulic works; underground aqueduct; Apulia region; ground-penetrating radar; electrical resistivity tomography

Introduction

In karst settings of the Mediterranean Basin and the Middle East, the need of water resources was faced in the earliest human settlements, due to the difficulties of finding water during the dry season. Many techniques were aimed at the storage of water in many ways, adapting to the local geomorphological and geological features of each specific site (Frumkin, 1999; Mays *et al.*, 2007; Parise *et al.*, 2013; Parise and Sammarco, 2015; Raikes, 1966; Teuma, 2005). Surface water supplies in karst areas are generally more limited than in other settings, which results in greater human dependency on groundwater than is the case in non-karst regions with similar climates (Aley, 2000; Parise and Gunn, 2007). Karst landscapes are typically characterized by lack or scarcity of surface water due to rapid infiltration into the soluble bedrock (Ford and Williams, 2007).

In southern Italy, several karst areas highlight the historic capability of humans to exploit water in order to facilitate human settlements. This was done by creating systems of transport and collection of the water and mostly underground storage. The use of the underground excavations to collect, transport and store water has a long history in this area of the world since Roman time with the most well known being underground and surface aqueducts to provide water to the main towns (Castellani and Dragoni, 1991; Hodge, 1992; Koloski Ostrow, 2001; Parise,

* Correspondence to: G. Leucci, CNR-IBAM, National Research Council of Italy. Institute for Archaeological and Monumental Heritage, Strada per Monteroni, Campus Universitario, Lecce, Italy.
E-mail: g.leucci@ibam.cnr.it

Received February 2015
Accepted February 2016

2011). Their construction indicates a high level of geological and hydrogeological knowledge reached by ancient populations (Del Prete and Parise, 2013.

The importance of these subterranean hydraulic works are being studied by a dedicated nationwide project by the Italian Speleological Society, which has resulted so far in the collection of information on more than 140 underground aqueducts throughout the country (Parise, 2009; Parise *et al*., 2009). The Apulia region contains 13 aqueducts, covering all the provinces, the longest being the Triglio aqueduct in the Taranto area, reaching some 18 km in total length (Delle Rose *et al*., 2006). The Triglio underground aqueduct was excavated in Roman times and supplied drinking water to the ancient town of *Tarentum* (Taranto).

Identification of the underground stretches of these hydraulic works can be extremely difficult if direct access is not possible (due to closure or destruction of the shafts, and to falls within the structure). In the last years several authors have used different geophysical techniques to explore for and map these features, with particular regard to ground-penetrating radar (GPR) (Bavusi *et al*., 2004; Chaminé *et al*., 2010; Galli *et al*., 2010; Leucci, 2004; Leucci *et al*., 2004; Leucci and De Giorgi, 2010; Nuzzo *et al*., 2004; Sammarco *et al*., 2010; Trogu *et al*., 2014). However, the GPR literature is for the most part lacking models for what complex void spaces of various geometries look like in reflection profiles and other images, so these studies are still in their infancy (cf. Conyers, 2012: 171)

The presented work illustrates the geophysical and archaeological surveys carried out in a short stretch of its route, located about 2 km south of the outskirts of Statte, at the north-eastern end of the property of the ILVA steel factory, the largest industrial facility in this part of Italy.

The studied sector is one of the few where the underground channel runs in a rural area, with presence of the aqueduct suggested by some shafts for ventilation and inspection. In particular; this area is at risk due to the project of expansion of the nearby so-called 'Mater Gratiae' quarry, within the ILVA property. Geophysical prospecting was performed to identify and document four vertical shafts and a total stretch of 400 m of horizontal aqueduct, with attention paid to the possible existence of secondary branches.

Geological and hydrogeological framework

The study area (Figure 1) is located within the southwest slope of the Murge plateau, where limestone and dolomitic limestone Cretaceous bedrock is overlain by Plio-Pleistocene calcarenites and clays (Martinis and Robba, 1971). Locally terraced, the slope descends from the plateau to the Ionian coastline and is incised valleys of fluvio-karst origin, locally known as *gravine* (Parise *et al*., 2003). The overall landscape, from the Murge plateau to the coast, is structurally controlled by faults and other tectonic discontinuities, which have produced the topographic relief.

The Triglio locality (Figure 1) is characterized by Plio-Pleistocene calcarenites that are up to 50 m thick, overlying the Cretaceous bedrock. Two water tables are present in the area, as in most of the Taranto province: a shallow aquifer, perched close to the surface by clay units within the calcarenites and the deeper water table within the Cretaceous limestones, sustained, according to pseudo-static equilibrium, by the nearby sea-level (Zorzi and Reina, 1962).

The construction of the Triglio aqueduct was predicated by an understanding of the position of shallow aquifer. Subsequently additional tunnels to intersect the water table created secondary branches in an effort to increase the water supply. The horizontal tunnel is characterized by having an arched ceiling, with an average height of 1.8 m. Vertical shafts were placed on the aqueduct path at distances of about 20 to 42 m between them. They performed several functions. During the initial construction of the tunnel they allowed work to proceed at several points and not just at the two faces at opposite ends of the tunnel. They were also useful in determining the depth of the tunnel below the surface, by dropping a plumb line down the shaft. This would also serve to determine and manage the slope of the tunnel. When the aqueduct was in use, the shafts provided air circulation and maintenance access.

The basic model for the aqueduct is that it taps into a shallow perched water table at higher elevations, within the unconsolidated Pliocene-age calcarenite. That water then flowed down one, and perhaps additional feeder aqueducts into the study area. It is possible that the upper reaches of the system also received water from the deeper water table found in the carbonate bedrock. However, by the time the water in the aqueduct reached the study area it was flowing at a depth much higher than the deeper water table.

Triglio aqueduct: the archaeological data

Taranto, which first developed in the eight century BC, was in origin one of the most prominent cities of Magna Graecia, founded by a group of Laconians along the Ionian coast. After falling into the orbit of Rome at the middle of the third century BC, Taranto, by the first century BC, had kept its cultural and agricultural

DOI: 10.1002/arp

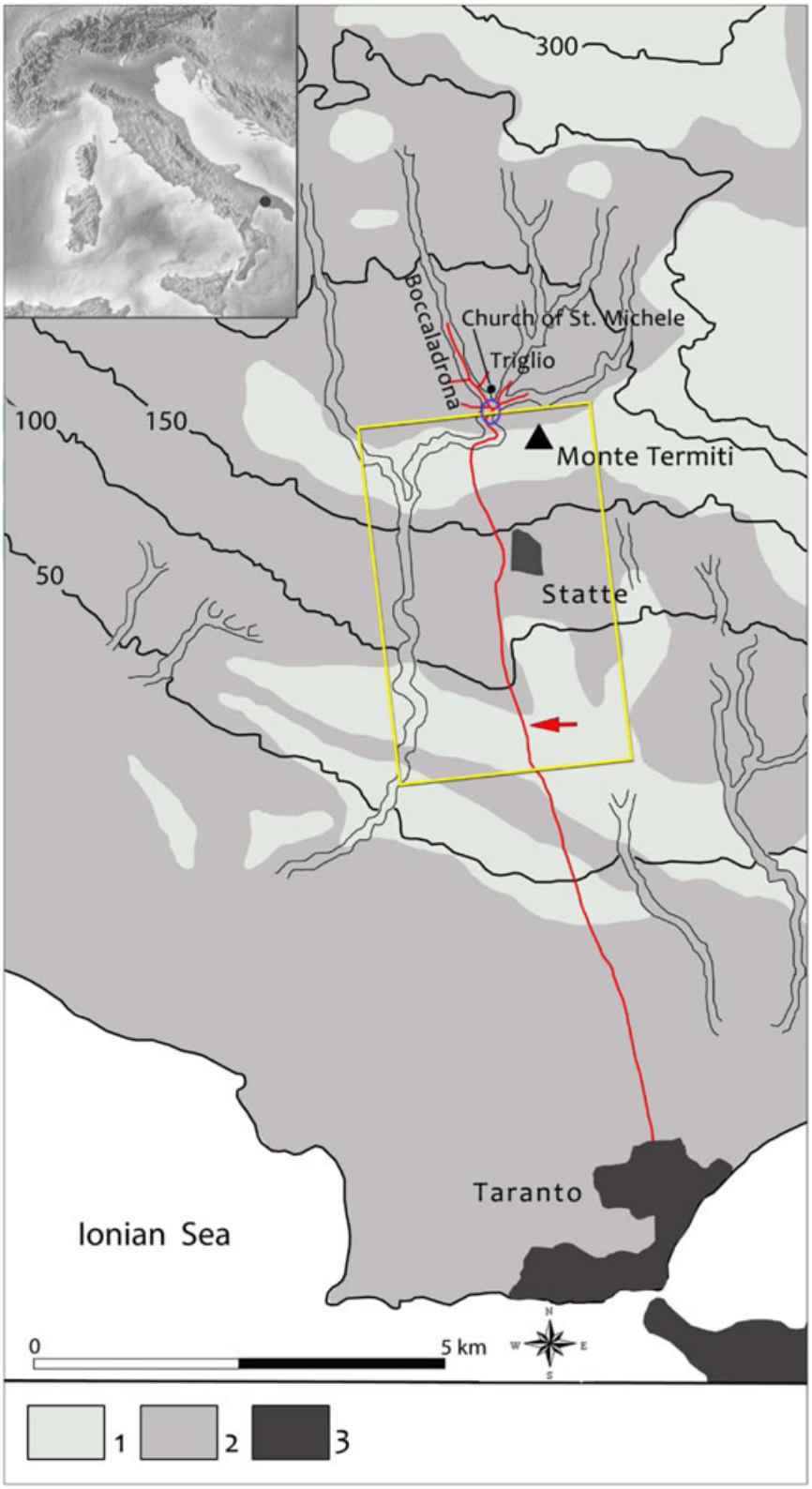

Figure 1. General setting and geological sketch map of the study area. The red line marks the supposed path of the roman underground aqueduct. Key: 1, limestones, dolomitic limestones; 2, calcarenites, clays; 3, urban areas. The blue circle indicates the location of the upper sector of the underground channel extensively explored during speleological surveys in Boccaladrona locality. The yellow square indicates the area shown in Figure 5; the red arrow indicates the stretch investigated through geophysical and archaeological surveys (see Figure 6).

DOI: 10.1002/arp

importance, for the production of wool, sea fruits and purple dye. Big and rich roman villas (*domus*) were built in pleasant positions, where the weather conditions were mild and ideal for leisure time (*otium*).

Cities of the Roman Empire were typically endowed with a basic infrastructure that included roads, bridges, public buildings, and aqueducts. As an important city, Taranto was certainly no exception. Two underground aqueducts supplied water to the Roman city: (i) the first, with origin in the Saturo Bay at the southern side of the city, was built during the first century BC and destroyed during the tenth century, and (ii) the second named Triglio aqueduct (after the locality where it has origin, on the southern slope of the Murge highplain) (Figure 2) at the northern side of the city.

Many archaeological problems remain concerning the chronology of the main underground channel of the Triglio aqueduct; some scholars assign its construction to Roman age (Becchetti, 1897), others date it to the Byzantine period (Fornaro, 1981). The final part of the aqueduct, 3 km-long, has an external course, marked by more than 200 arches, and was built in its monumental shape during the fourteenth century AC. The great importance of this hydraulic infrastructure required the continuity in its use until AD 1928 and several restoration works of the aqueduct, which is still in use for agricultural irrigation.

Only a few hundred metres of the aqueduct have been explored at the Boccaladrona locality (Figure 1) (Gentile and Ficocelli, 2008). A part of the horizontal tunnel has been extensively explored by cavers. It consists of a gallery entirely dug in the local stone, about 6 m below the ground surface. Some sectors of the ceiling and walls were reinforced by small blocks of limestone during the the fifth and tenth centuries AC (Figure 3).

Figure 2. Historical map (*Carte topographique de la ville et des environs de Taranto*, 1801), showing the path of the ancient aqueduct in the upper and middle part of its course (from http://www.geog.queensu.ca/napoleonatlas/Introduction/M.13.C.00.595_small.htm).

Figure 3. Views of the underground *specus* explored during speleological survey in Boccaladrona locality: (a) the left wall of the tunnel, reinforced by small blocks of limestone, is evident; (b) a sector of the channel entirely carved in local stone.

DOI: 10.1002/arp

The horizontal aqueduct is about 70 cm wide and 140–200 cm high. Vertical shafts about 80 cm × 80 cm in width (Figure 4) were placed about 40 m apart (Grassi *et al.*, 1991). Some shafts are well preserved, allowing entrance and exploration, while others are clogged by detritus or collapsed blocks of rock.

Geophysical surveys

Fieldworks in the surveyed area: planning of measurements and positioning in a digital map

Before performing geophysical measurements, archaeological field-walking of the area and topographical surveys of the ancient remains were conducted (Figure 5). In particular, four vertical shafts were identified and the possible route of the aqueduct was mapped between them (labelled 1, 2, 3 and 4 in Figure 6). Figure 7 shows the surface evidence for the vertical shafts and their interior. Taking into account the distance between the four shafts (in particular, between the first and the second, and between the third and the fourth, respectively) it is likely there is another shaft, not visible today between shafts 3 and 4. Considering their position, it is possible to hypothesize a stretch of the aqueduct, about 400 m long, with northwest–southeast (NW–SE) direction, today crossed by the road (Figure 6).

The study area contains many fallen trees and the ground surface is uneven (Figure 8) allowing the placement of only a few GPR profiles. In order to understand the bedrock stratigraphy and correlate units to GPR profiles an electrical resistivity tomography (ERT) survey was conducted just to the west of the hypothesized aqueduct.

The following instrumentation of the Geophysical Laboratory for Archaeology of the Institute for Archaeological and Monumental Heritage (CNR-IBAM) in Lecce was used: a GPR Hi Mod model equipped with 200 and 600 MHz dual band antennas, a Syscal Kid Resistivity-meter with 24 active channels, and a GPS Sokkia GRS2700ISX.

Seven GPR profiles (Figure 6, R1–R7) were collected where the ground conditions were suitable. An area of approximately 115 m × 177 m to the west of the route of the aqueduct was surveyed with the ERT system for stratigraphic correlation (Figure 6, A).

ERT prospecting

ERT data were acquired in a grid 115 × 177 m^2 using a dipole–dipole array. The electrodes distance was 4 m and the grid step was 4 m. The aim of ERT measurements was to obtain significant information related to both the presence of archaeological features in the investigated area, in those sectors where it was not possible to use the GPR method and to identify the bedrock depth. ErtLab software (Geostudi Astier and Multi-Phase Technologies, 2013) was used in order to obtain a three-dimensional (3D) resistivity distribution in the subsoil. Its numerical core was based on tetrahedral Finite Elements (Munjiza, 2004). This algorithm is more adapt for inversion of 3D data.

For two-dimensional (2D) data inversion the Res2Dinv software applying Loke and Barker inversion methods. The software employs a quasi-Newton technique to reduce the numerical calculations (Loke and Barker, 1996). It produces a 2D resistivity model satisfying measured

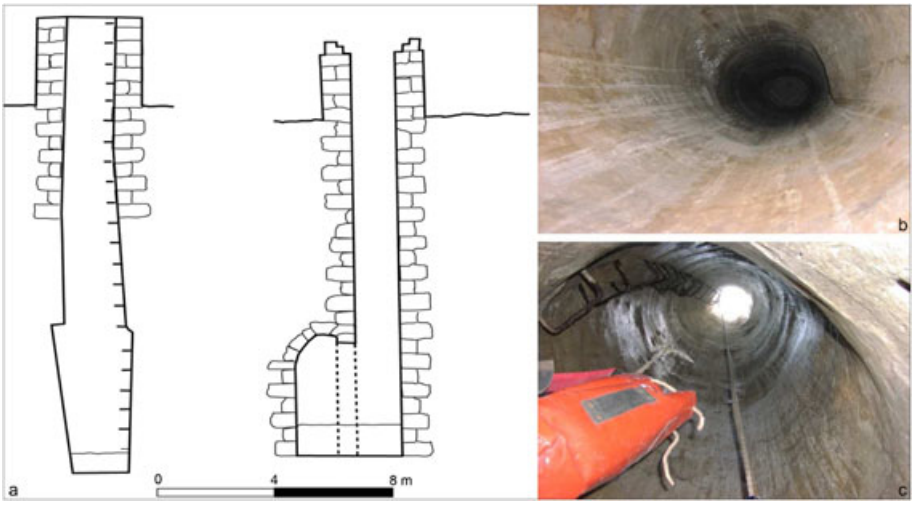

Figure 4. (a) Cross-sections of two different sectors of the main channel in Boccaladrona locality with opened vertical shafts (modified after Gentile and Ficocelli, 2008); (b) and (c) interior views of ventilation shafts from the Boccaladrona main channel.

DOI: 10.1002/arp

Figure 5. Satellite image taken in 2013, showing in red the route of the Triglio aqueduct; the arrow indicates the stretch investigated through geophysical and archaeological surveys.

data in the form of a pseudo-section. The goodness-of-fit is expressed in terms of the relative root mean square (RMS) error. This method is more suitable where both strong lateral resistivity variations and depth changes occur and in complex geological models such as in a karstic area (Leucci, 2004).

A typical image from the 2D ERT survey is shown in Figure 9. It shows a layered resistivity profile in the top 6 m as a zone of relatively low resistivity (about 180 to 400 Ω m), labelled 'L' from the surface to about 1.0 m depth. This unit overlies a medium resistivity zone labelled M (about 900 to 1500 Ω m). The upper resistivity layer is undulating and its depth ranges from between 1.0 and 3.5 m. The lower layer, labelled H (Figure 9), is characterized by high resistivity values ranging between 2000 and 3500 Ω m. The geological model established by means of a 2D resistivity imaging profile (Figure 9), allows for three different zones to be detected: covering materials (layer 'L') consist of soil mixed with calcarenite that is weakly cemented; Plio-Pleistocene calcarenites and clays (layer 'M'); dolomitic limestone Cretaceous bedrock (layer 'H').

Lateral discontinuities, labelled 'C', 'D' and 'E' represent low resistivity zones surrounding by high resistivity. These zones likely consists of soil-filled karst features (Leucci, 2004; Leucci *et al*., 2004).

The 3D resistivity model by depth slices is shown in Figure 10. There is a general increase of resistivity values with depth. The uppermost slice (0.5–1.0 m in depth) shows a larger area with high resistivity variations over short distances (about from 150 to 1500 Ω m). In comparison, slice 2, lying at a depth ranging from 2.0 to 2.5 m, shows more gradual lateral variations in the model resistivity values; here, resistivity values of about 1500 and 2000 Ω m are clearly visible. The resistivity values increase in the slices 3 (3.0–3.5 m in depth) and 4 (8.0–8.5 m in depth). The 3D resistivity model shows the geometry of the geological stratigraphy and clearly confirm the results of 2D resistivity model.

Since defining the site stratigraphy a GPR profile R7 was acquired in order to adjoin the ERT grid. The GPR profile (Figure 11a and 11b) and corresponding resistivity section (Figure 9) exhibit a number of similarities. In particular a shallow layer of sediments sits on bedrock (yellow dashed line). This uppermost unit displays numerous reflections ('B') attributable to perhaps sedimentary units or clasts sitting on contact with the underlying bedrock. This layer has a thickness variable between 0.4 and 2.5 m. Within the same regions of the profile, amplitude reflections ('C') indicate the presence of soil-filled karst features, with discontinuities along reflection horizons potentially indicating fractures.

Comparing with the ERT profile (Figure 9) it is possible to note the bedrock at a depth ranging between 0.8 and 2.5 m. The reflection events 'D' and 'E' are probably related to the presence of an area filled with soil (Figure 11b). In fact they are comparable with the resistivity anomalies labelled 'D' and 'E' in Figure 9.

GPR prospecting

The GPR profiles were normalized for amplitude, had background removed and were migrated using a Kirchoff 2D method.

DOI: 10.1002/arp

Figure 6. General map of the investigated area, showing in red the route of the Triglio aqueduct and the location of the shafts 1–4, in yellow the GPR profiles R1–R7, and in light blue the area surveyed using electrical resistivity tomography (ERT) (A).

Figure 7. Shaft 1 with the underground tunnel (a) and the external structure of shaft 2 (b).

Figure 8. Photographs that show the site condition.

DOI: 10.1002/arp

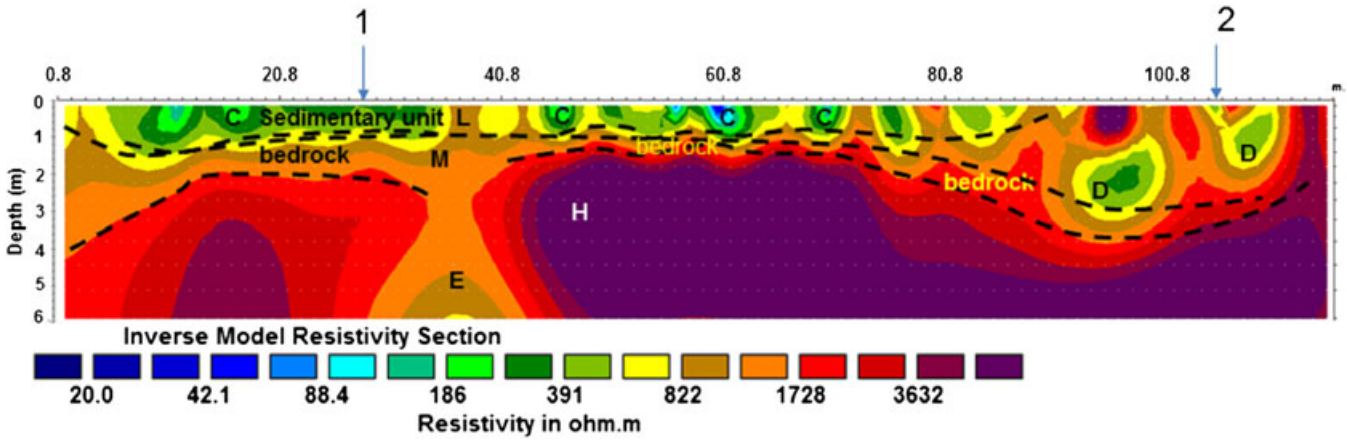

Figure 9. Two-dimensional (2D) distribution of resistivity; H, high resistivity values (2000–3500 Ω m); L, low resistivity values (180–400 Ω m); M, medium resistivity values (900–1500 Ω m). C and D corresponds to the soil-filled karst features. The numbers 1 and 2 indicate the position of R1 ground-penetrating radar (GPR) profile (1 is the start and 2 is the end).

In order to perform a 2D Kirchoff migration the electromagnetic (EM) wave velocity was determined from the reflection profiles acquired in continuous mode, using the characteristic hyperbolic shape of reflection from a point source (Fruhwirth *et al.*, 1996). This is a very common method of velocity estimation and it is based on the phenomenon that a small object reflects EM-waves in almost every direction. The general stratigraphy in all profiles shows an unconsolidated surface soil with many stones that produced point-source reflections, as well as a few metal objects (Figures 11–16) that enabling EM-wave velocity analysis to be performed. The processing and imaging software (Sandmeier 2013 Reflex) allows the interactive velocity adaptation of a diffraction or reflection hyperbola by calculating a hyperbola of defined velocity and
F11–16 width. The velocities are combined into a 2D model using a special interpolation method. The interpolation is performed as follows: all actual velocities are summed for every point in the x–t range, proportional to the square of their distance from the (x, t) point. This method provides only the average EM-wave velocity to the depth of the source-point reflector. This type of 2D velocity distribution may be used in the 2D migration processing step. Application of this method gives both vertical (in time, hence in depth) and lateral velocity variations from 0.05 m/ns to 0.11 m/ns Yilmaz, 1987. An average velocity of 0.08 m/ns is obtained over the survey area.

R1 profile was acquired to cross the horizontal Triglio aqueduct (Figure 6) whose position was estimated by connecting the locations of the vertical shafts. In fact the reflection event labelled 'A1' (between two vertical dashed yellow lines) is likely the vertical shaft, filled with debris (Figure 13). These complex reflections generated within the shaft were produced by the sediment and/or rubble that fills this incision. This feature was detected at the correct depth in the profile.

As a confirmation of the reflective nature of an arched ceiling of the aqueduct a 2D model was produced using GPR-Sim (Goodman, 2013).

This program allows the user to generate a synthetic model of what might be expected using known properties of the ground and the geometry of underground features (Conyers, 2013). A model of a stratified subsoil with the presence of a void related to the aqueducts and a soil-filled karst feature was assumed (Figure 12). Two homogeneous layers with a dielectric constant of 16 and 9 were modelled for the calcarenite and hard bedrock, respectively. In the bedrock a void space, with dielectric constant of one, represents the aqueduct ceiling. A soil-filled karst feature, with a dielectric constant of 20, was placed at the contact between the two modelled layers.

The synthetic reflections demonstrated that the aqueduct ceiling arch would generate reflection when energy intersected the void space, as was expected. The floor of this feature also generated an upward bowing reflection from the velocity 'pull up' in the void space. Other reflection events were generated at the contact between soil 4 and 7 with lower amplitude reflections produced from the soil-filled karst features.

When this model was compared to the reflection profile R1, all the modelled reflections were visible. Looking at Figure 13a (600 MHz reflections), a contact between Plio-Pleistocene calcarenites and bedrock, labelled 'B' is visible. This reflection event is visible at variable depth between 0.4 and 0.8 m. Numerous reflections between the abscissa 0–12 m and 0.8–2.4 m in depth, labelled 'V', are probably soil filled karst

DOI: 10.1002/arp

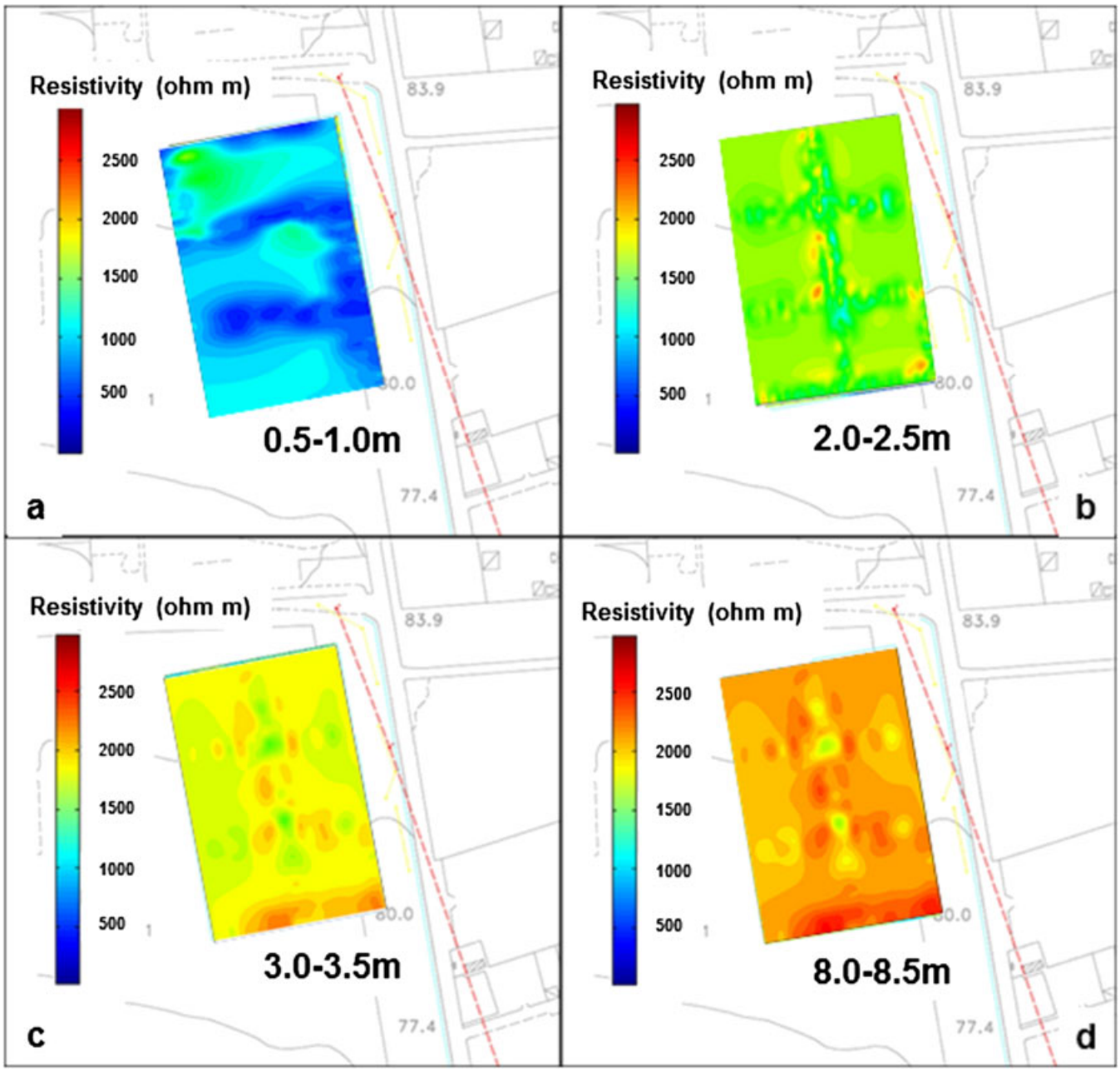

Figure 10. Three-dimensional (3D) distribution pattern of resistivity at depths 0.5–1 m (a), 2–2.5 m (b), 3–3.5 m (c), and 8–8.5 m (d).

features such as the reflections at the abscissa 18–32 m and 0.8–2.8 m in depth.

As visible in Figures 13a and 13b the reflections visible at the abscissa 16–18 m and depth of about 2.4 m are the aqueduct ceiling. Also the aqueduct floor is visible as velocity pull up reflection in the 200 MHz antenna profile (Figure 13b). The 200 MHz profile (Figure 13b) produces an even better image of the features here, as there is less clutter. The higher frequency energy (600 MHz) was attenuated before it could be transmitted to the floor of the aqueduct and that feature remains invisible with those data images.

With the aim of strengthening the interpretation made for the R1 profile the single reflection traces were analysed. When radar energy is reflected from a buried interface where the wave velocity decreases, the polarity of the reflected wave will be the same as the direct-wave generated from the transmitting antenna. This is the normal case in most ground

DOI: 10.1002/arp

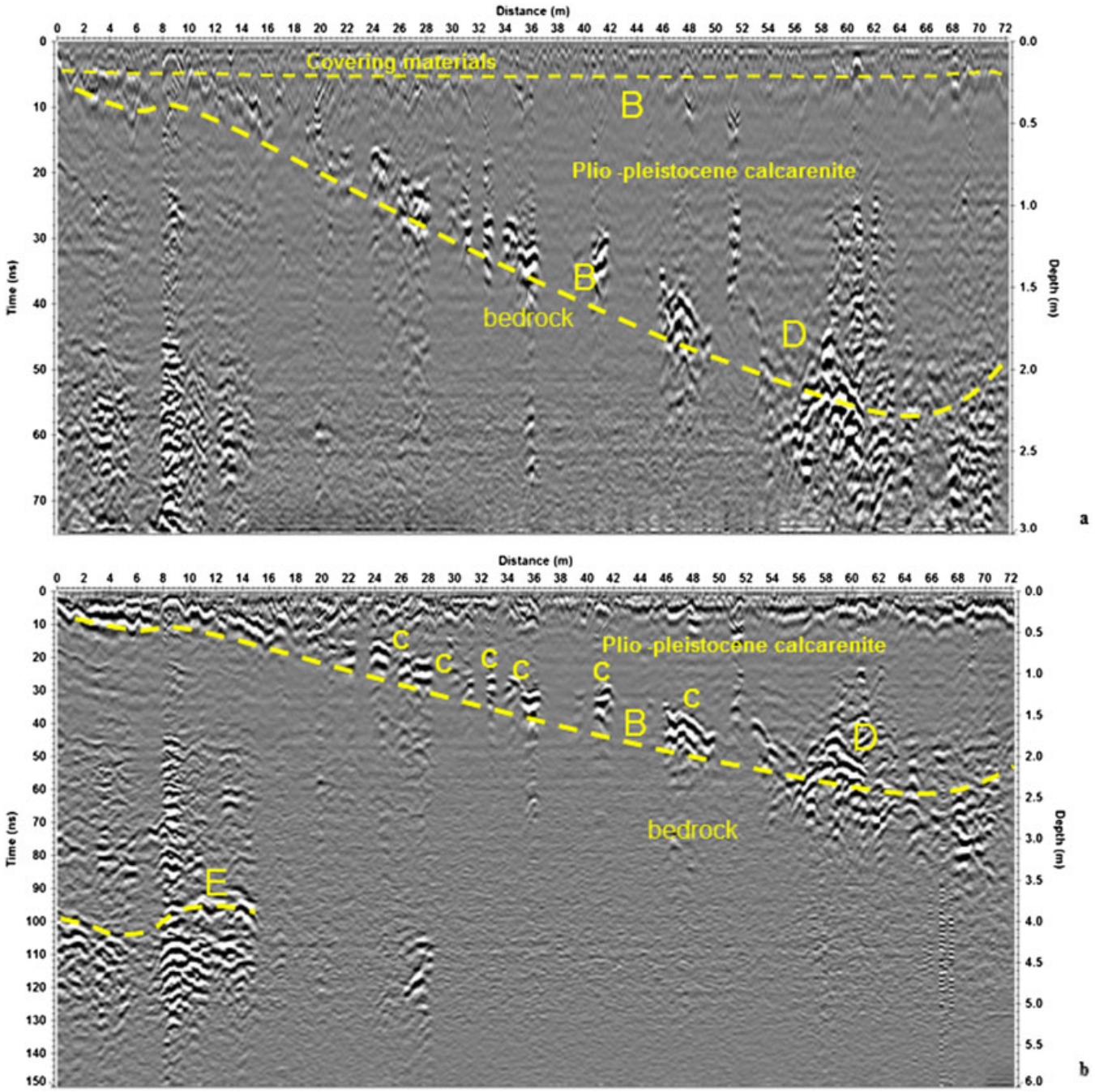

Figure 11. Radar cross-section along the profile R7 [600 MHz (a); 200 MHz (b)], in which some reflection events are highlighted that were interpreted as due to the layered geology ('B') and several reflection events ('C', 'D', and 'E') interpreted as owing to soil filled karst features.

conditions, and therefore, most reflections are recorded as normally polarized sine waves (Conyers, 2015a, 2015b). However, if a drastic increase in velocity occurs at a boundary, such as a void space where propagating radar waves increase again to the speed of light, a reflection will be generated that is visible in traces as a reversed polarity sine wave (Conyers, 2015a, 2015b).

Discontinuities along banded reflections may indicate the presence of joints or fractures. A mottled reflection pattern may indicate fractured bedrock or soil or that gravel fill materials are present that scatter EM energy. In instances where cavities/voids/caves were interpreted as present, due to the resonance of the EM energy within the void and likely irregular and unknown shape of the bottom of these features,

DOI: 10.1002/arp

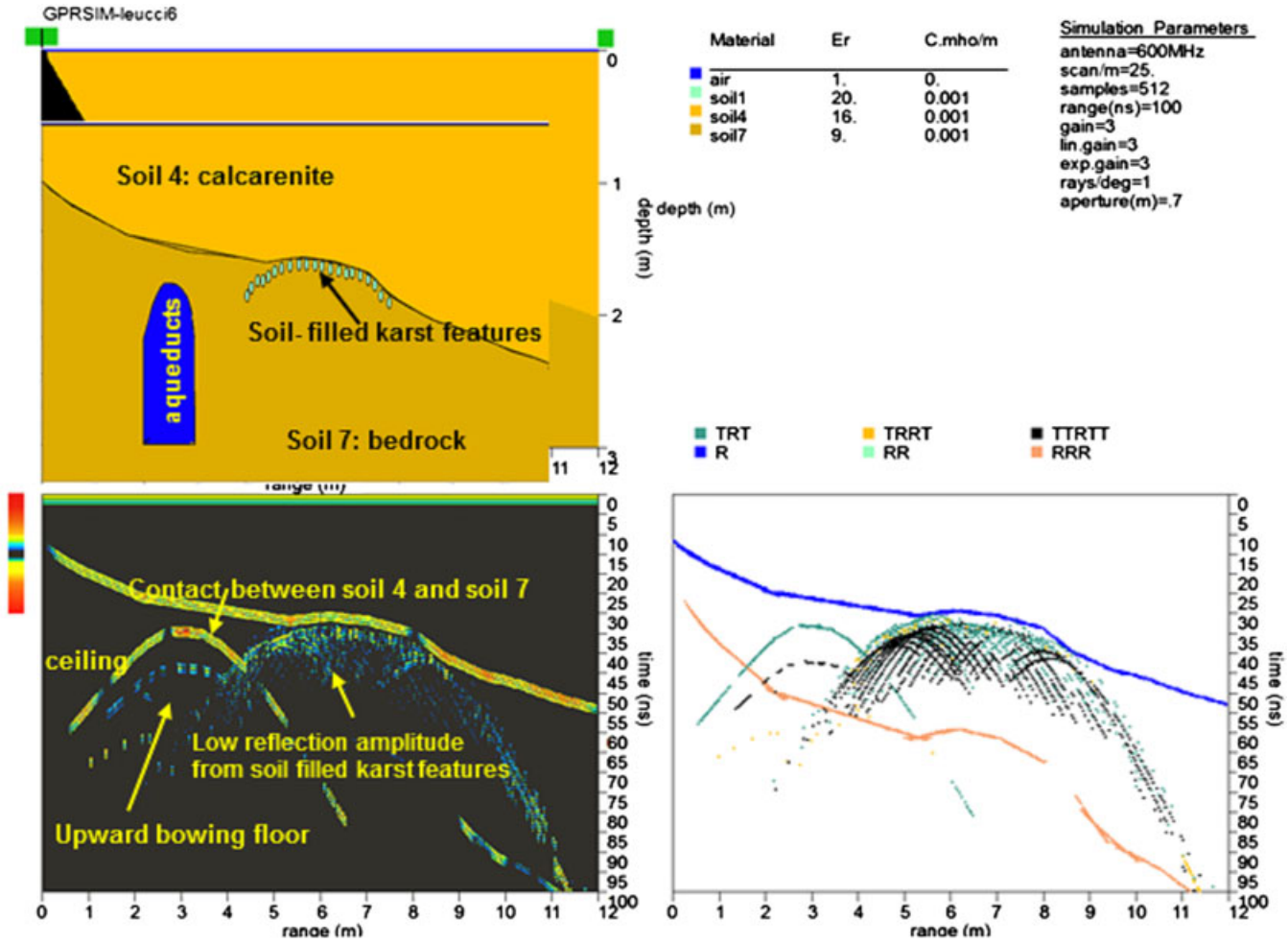

Figure 12. Forward model: two homogeneous layers with a dielectric constant of 16 and 9 were modelled for the calcarenite and hard bedrock, respectively. In the bedrock a void space with dielectric constant of one, represents the aqueduct. A soil-filled karst feature, with dielectric constant of 20, was placed at the contact between the two hypothesized layers.

the horizontal extent and depth to the upper interface of bedrock and void were most discernable.

Usually, as radar energy moves deeper into the ground, moisture retention increases and EM wave velocity will decrease. When radar energy is reflected from a buried interface where the EM wave velocity decreases, the polarity of the reflected wave will be the same as the direct-wave generated from the transmitting antenna (Conyers, 2015a, 2015b). This is the normal case in most ground conditions, and therefore, most reflections are recorded as normally polarized sine waves. If a drastic increase in velocity occurs at a boundary, such would occur when waves enter a void space and move at the speed of light, a reflection will be generated that is visible in traces as a reversed polarity sine wave (Conyers, 2015a, 2015b).

Figures 14a and 14b show the trace reflections and illustrate the difference between reflections generated from the soil filled karst feature (Figure 14a) and the ceiling of the aqueduct (Figure 14b). The change of polarity to a reversed polarity reflection at this feature is confirmation that this feature is the bedrock–air interface at the aqueduct ceiling. The reflection from the nearby soil-filled karst features exhibits normal polarity.

R3 profile was collected sub-parallel to the presumed orientation of the aqueduct, and crossed it only at its end. In the R3 profile two reflection events 'A1' and 'A2' (yellow boxes in Figures 15a and 15b), were near shaft 2 (Figure 6). They show the same truncation of the bedrock as shown in Figures 13a and 13b the one above, where the shafts are also filled with sediment. The two similar reflection events 'A1' and 'A2' are probably related to one shaft and were displayed twice as the profile was collected to the side of this vertical feature and there were two very different pathways

DOI: 10.1002/arp

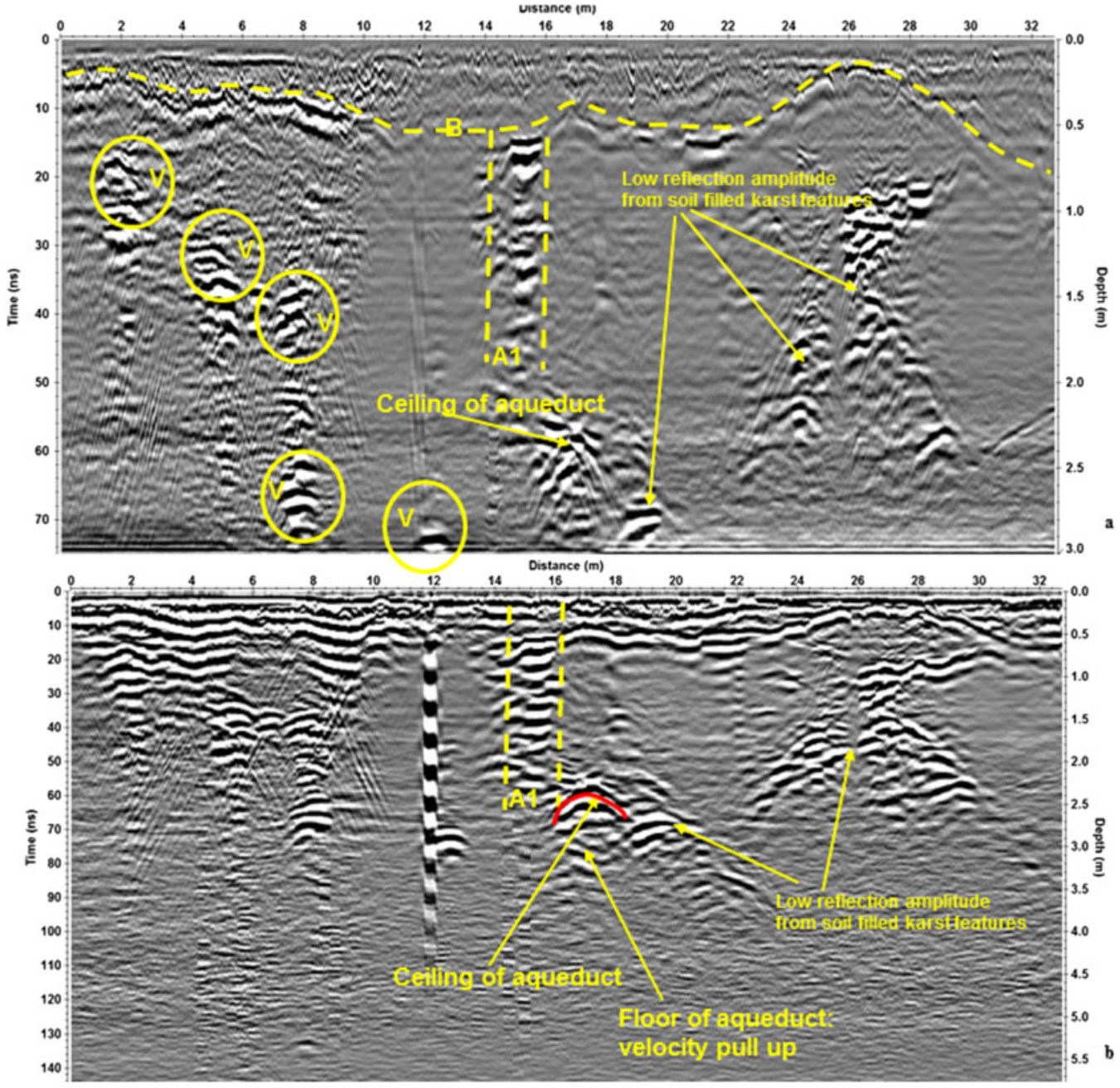

Figure 13. Radar cross-section along the profile R1 [600 MHz (a); 200 MHz (b)], in which some reflection events are highlighted that were interpreted as a vertical shaft filled with materials (A1), the ceiling and floor of the Triglio aqueduct, the contact between the Plio-Pleistocene calcarenite and the bedrock (B), some soil-filled karst feature within the bedrock (V).

of energy going to and from it, both of which were imaged. This double-recording of one feature is highly unusual, but illustrates how radar energy can travel preferentially in multiple pathways at oblique angles to and from vertical reflection surfaces of this sort. An alternative hypothesis is that there are actually two vertical shafts in this area, one of which may have collapsed and had to be abandoned, and the second shaft was then re-excavated. It is not known which of these is the case here.

The reflection events labelled 'B1' and 'B2' are related to two unit boundaries: 'B1' is the contact between covering materials and Plio-Pleistocene calcarenites; 'B2' is the contact between Plio-Pleistocene calcarenites and bedrock. The reflection event 'B2' is visible only in the second part of the profile (abscissa 16–30 m). This could

DOI: 10.1002/arp

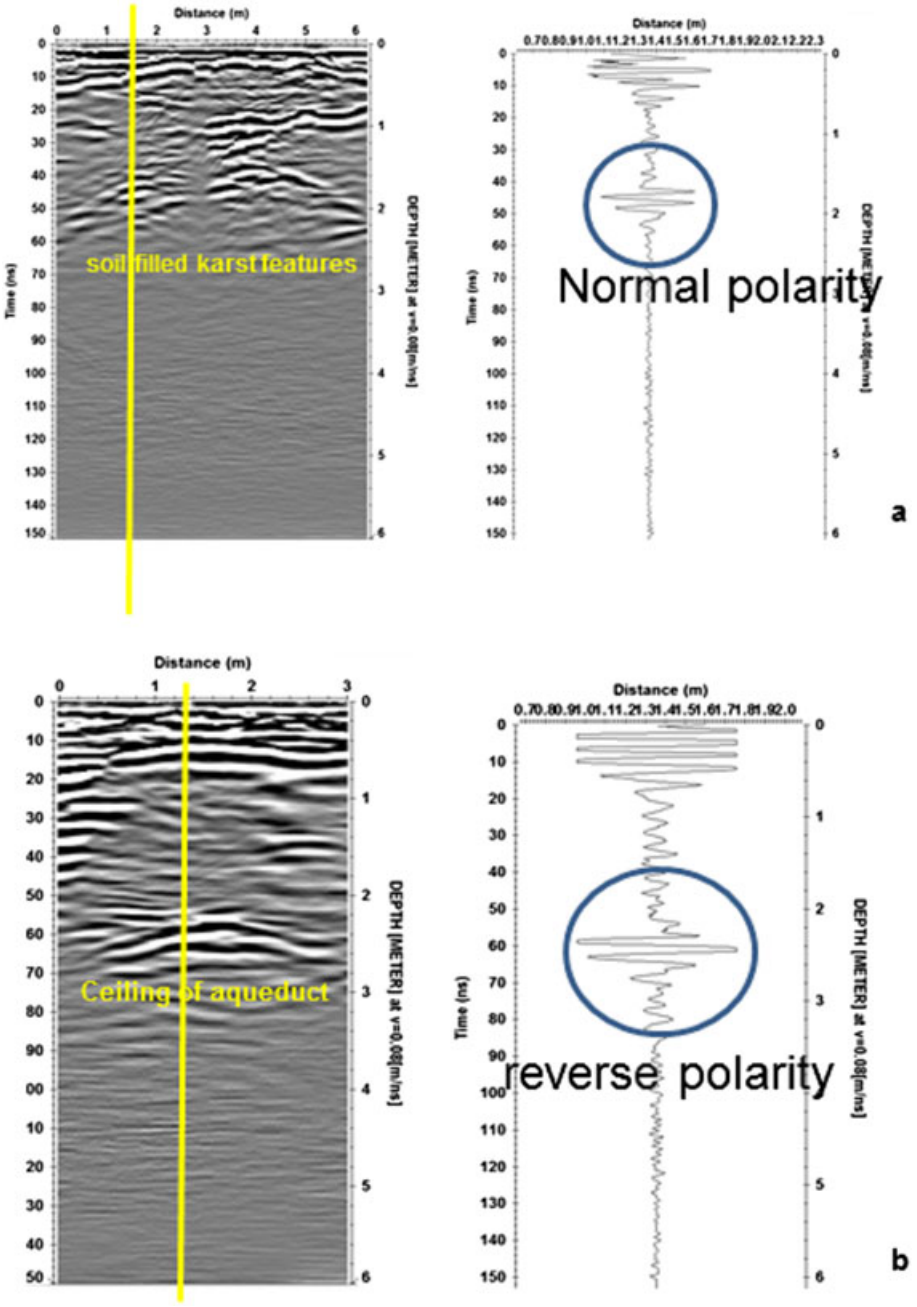

Figure 14. Comparison of reflection traces from waves reflected from soil-filled karst feature (a) and aqueduct ceiling (b). The usual case for most buried materials produces reflections that are normal polarity (a). In burials that retain void spaces, reflections are reversed polarity (b).

be due to the high radar energy attenuation in the first part of the profile.

The most interesting reflections in this transect (Figure 15b) are those produced from the 200 MHz energy. The radar energy from this antenna travelled farther in the ground and was reflected off the aqueduct ceiling in a number of locations. As the profile transect is almost parallel to the inferred orientation of the aqueduct, the ceiling reflections were recorded as a slightly undulating fairly low amplitude reflection (indicated by A3 on a yellow dashed line). It is likely that only a few areas in the aqueduct ceiling contain surfaces oriented in a way to reflect energy obliquely back to the surface antenna, and therefore this surface is variable in the way it was recorded in a reflection profile. This important anthropogenic

DOI: 10.1002/arp

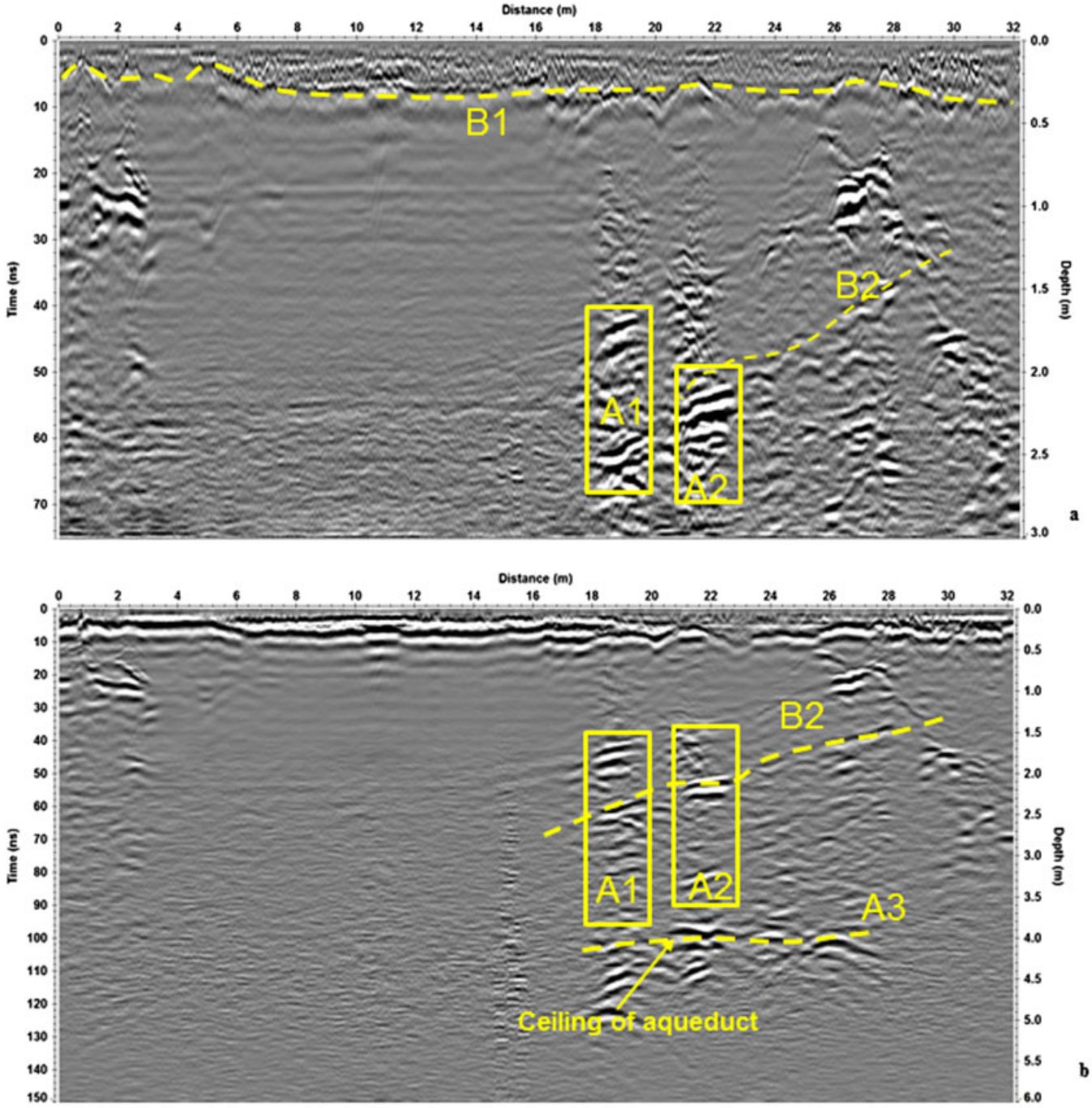

Figure 15. Radar cross-section along the profile R3 [600 MHz (a); 200 MHz (b)], in which some reflection events are highlighted that were interpreted as owing to the vertical shaft (A1, A2) and layered underground (B1 and B2); moreover, a weak, slightly undulating, reflection, perhaps connected to the ceiling of the aqueduct is indicated (A3).

feature could be confused for a natural bedrock feature if the location of the aqueduct was not known from the vertical shafts and other GPR profiles. A calculation of the distance that radar energy travelled to and from the surface antenna at an angle correctly places this reflection at 110 ns (Figure 15b).

R4 profile (Figure 16) also crosses the aqueduct (abscissa 0–4 m).

The reflection feature labelled 'A' (yellow box in Figure 16a) is similar to the aqueduct ceiling reflection in profile R3 (Figure 15). The vertical shaft leading to the horizontal aqueduct is also visible.

DOI: 10.1002/arp

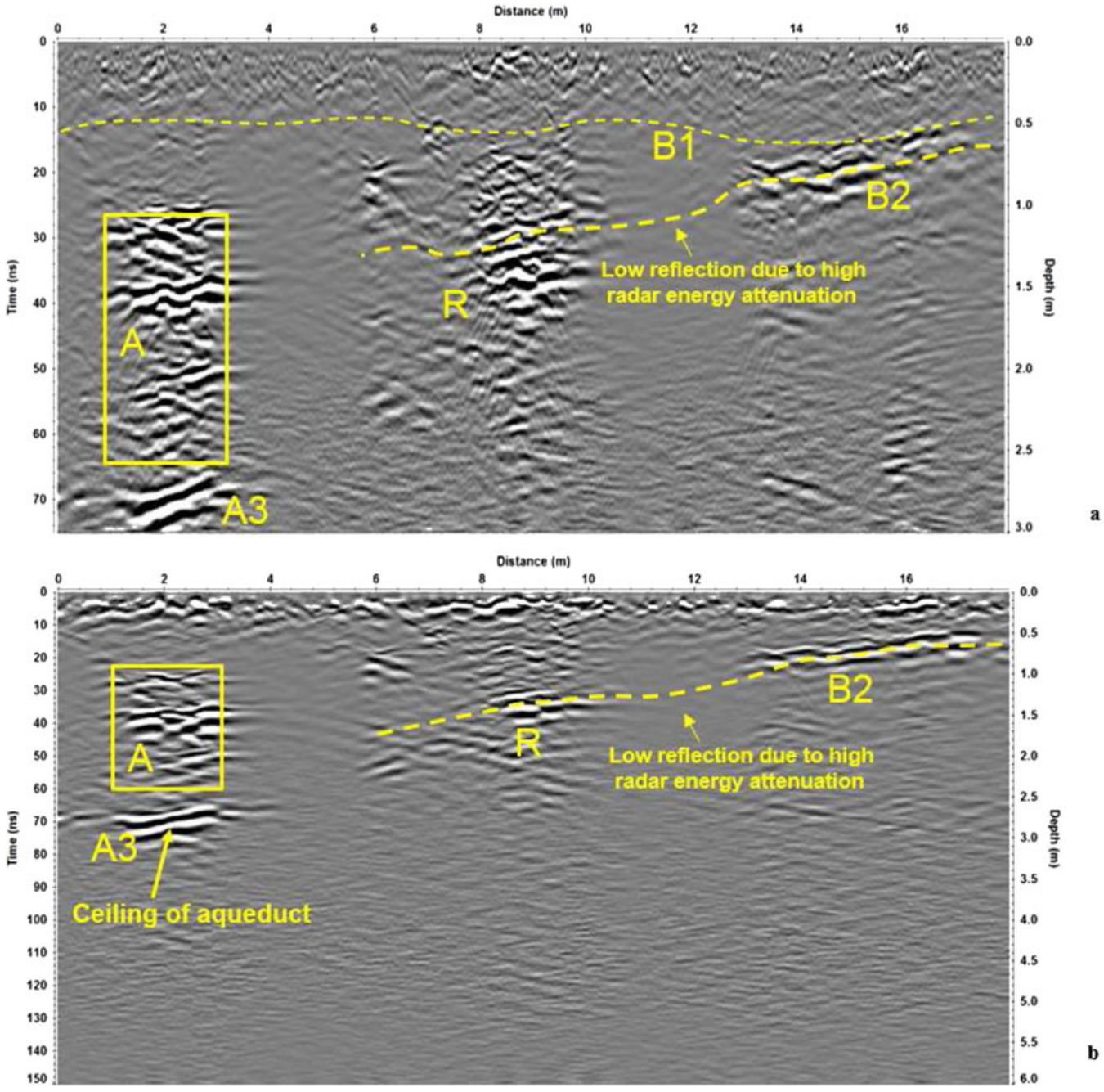

Figure 16. Radar cross-section along the profile R4 [600 MHz (a); 200 MHz (b)], in which some reflection events are highlighted that were interpreted as owing to the shaft (A), layered underground (B1 and B2), and soil-filled karst feature (R).

Also in this case the reflection event 'A3' is related to the ceiling of the aqueduct. In fact at this point the profile crossed the projected aqueduct. A calculation of the distance that radar energy travelled to and from the surface antenna at an angle correctly places this reflection at 70 ns (Figures 16a and 16b). The reflection event 'R' could be interpreted as a soil filled karst void.

The reflections labelled 'B1' and 'B2' are related to the two contacts: the first one 'B1' is the contact between covering materials and Plio-Pleistocene calcarenites; the second one 'B2' is the contact between Plio-Pleistocene calcarenites and bedrock. The reflection event 'B2' is partially visible due to the high radar energy attenuation in the upper part of the profile.

DOI: 10.1002/arp

Archaeological interpretation

The geophysical surveys were aimed at obtaining a model for two features of archaeological interest, the aqueduct and the vertical shafts leading to it. It was also a goal of this study to differentiate these important features from fractures and natural cavities filled with sediment in the bedrock. An integration of the ERT and GPR methods was also important in order to understand the stratigraphy and allow for the identification of unit reflection profiles.

Much complexity in reflections resulted from the presence of a non-homogeneous bedrock and fractures in the rock. The important reflection features of the shafts and aqueduct were found in profiles R1, R3 and R4 (see Figures 11, 13 and 15). It is important to note that only in profile R1 did the aqueduct ceiling match exactly what the forward model predicted (Figure 12). That is because only this profile crossed the underground void at an angle approaching perpendicular. Elsewhere the ceiling was still visible, however, as a high amplitude reflection that was roughly horizontal when profiles were parallel to the aqueduct and not directly on top of it. Its origin could be confirmed by an analysis of the polarity changes in individual traces, and also a calculation of its expected depth from a knowledge of the radar travel velocity in this area.

Conclusions

The work highlights the importance of the integration of different research methods for the study of ancient underground structures. In particular, archaeological and topographical surveys allowed the identification and the accurate reconstruction of the route of the Triglio aqueduct thanks to the documentation and positioning of some shafts and the analysis of the tunnel. These investigations allowed the planning of geophysical prospecting according to the tasks of the research, the geological characteristics of the study area and the ground conditions. Geophysical surveys were based on the integration of two different methods, GPR and ERT, which allowed a very effective system of investigation aimed at the documentation of a stretch of the underground work. The GPR reflections are very complicated in this area and those generated from the aqueduct and the debris-filled vertical shafts could be easily confused with natural karst features or bedrock fractures. Forward modelling helped to understand the nature of reflections of interest and an analysis of individual traces could confirm the reversed polarity caused by a void space reflection. Only an intuitive understanding of generated reflection profiles and traces can produce important clues during these types of complicated interpretation tasks. In addition the variability of aqueduct ceiling reflections and a variety of reflections generated from the edges and irregularities at this interface could be possibly identified with ERT results and then confirmed with individual trace reflection analysis and forward modelling

The 200 MHz antenna data were fundamental in order to better understand the aqueduct structure. In fact in more deeply buried void spaces only this lower frequency energy had the penetration necessary to intersect the feature. In most shallower units the 200 MHz reflection profiles showed almost the same features as the 600 MHz, but with far less resolution.

Acknowledgements

The authors are grateful to Drs Lara De Giorgi and Fabio Fortinguerra (CNR-IBAM), and to Officine di Levante s.r.l. for their support during the fieldwork, and to Giacomo Di Giacomo for processing and management of geographical data.

The authors are grateful to Professor Lawrence Conyers for his valuable suggestions that have improved the paper.

References

Aley T. 2000. Water and land-use problems in areas of conduit aquifers. In Speleogenesis. Evolution of karst aquifers, Klimchouk AB, Ford DC, Palmer AN, Dreybrodt W (eds). National Speleological Society: Huntsville, AL; 481–484.

Bavusi M, Chianese D, Giano SI, Mucciarelli M. 2004. Multidisciplinary investigations on the Roman aqueduct of Grumentum (Basilicata, Southern Italy). *Annals of Geophysics* **47**: 1791–1801.

Becchetti S. 1897. Acquedotto di Triglio. In Antico acquedotto romano delle Acque Ninfali, Becchetti S (ed). Tipografia fratelli Martucci: Taranto.

Castellani V, Dragoni W. 1991. Italian tunnels in antiquity. *Tunnels & Tunneling* **23**(3): 55–57.

Chaminé HI, Afonso MJ, Robalo PM, *et al.* 2010. Urban speleology applied to groundwater and geo-engineering studies: underground topographic surveying of the ancient Arca D'Água galleries catchworks (Porto, NW Portugal). *International Journal of Speleology* **39**(1): 1–14.

Conyers LB. 2012. Interpreting Ground-penetrating Radar for Archaeology. Left Coast Press: Walnut Creek, CA.

Conyers LB. 2013. Ground-Penetrating Radar for Archaeology 3rd Edition. Alta Mira Press 258 pp.

Conyers LB. 2015a. Analysis and interpretation of GPR datasets for integrated archaeological mapping. *Near Surface Geophysics* **13**: 645–651.

Conyers LB. 2015b. Ground-penetrating radar data analysis for more complete archaeological interpretations.

DOI: 10.1002/arp

Proceedings of the 11th International Conference on Archaeological Prospection, 15–19 September, Warsaw, Poland. *Archaeologia Polona* **53**: 202–205.
Delle Rose M, Giuri F, Guastella P, Parise M, Sammarco M. 2006. Aspetti archeologici e condizioni geologico-morfologiche degli antichi acquedotti pugliesi. L'esempio dell'acquedotto del Triglio nell'area tarantina. *Opera Ipogea* **1–2**: 33–50.
Del Prete S, Parise M. 2013. An overview of the geological and morphological constraints in the excavation of artificial cavities. In *Proceedings 16th International Congress of Speleology*, Filippi M, Bosak P (eds), Brno, 21–28 July, volume 2, 236–241.
Ford D, Williams PW. 2007. Karst Hydrogeology and Geomorphology. John Wiley & Sons: Chichester.
Fornaro A. 1981. Provincia di Taranto. Ricerche sull'assetto del territorio. : Manduria publisher.
Fruhwirth RK, Schmoller R, Oberaigner ER. 1996. Some aspects of the estimation of electromagnetic wave velocities. In *Proceedings of the 6th International Conference on Ground Penetrating Radar*, Tohoku University, Sendai, Japan; 135–138.
Frumkin A. 1999. Interaction between karst, water and agriculture over the climatic gradient of Israel. *International Journal of Speleology* **26B**(1/4): 99–110.
Galli PAC, Giocoli A, Naso JA, *et al.* 2010. Faulting of the Roman aqueduct of Venafrum (southern Italy): methods of investigation, results, and seismotectonic implications. *The Geological Society of America, Special Paper* **471**: 233–242.
Gentile GC, Ficocelli S. 2008. Lavori di recupero nell'acquedotto del Triglio (Taranto, Puglia) e monitoraggio delle acque. *Opera Ipogea* **1–2**: 179–184.
Geostudi Astier s.r.l. and Multi-Phase Technologies LLC. 2013. ErtLab Software via A. Nicolodi, 4857121 Livorno.
Grassi D, Zerruso F, Pascali E, Giliberto M. 1991. Indagine sull'acquedotto del Triglio. Note preliminari. *Itinerari Speleologici* **5**: 173–176.
Goodman D. 2013. GPR Sim Manual. http://www.gpr-survey.com (accessed June 2013).
Hodge AT. 1992. Roman Aqueducts and Water Supply. Duckworth Archaeology: London.
Koloski Ostrow AO (ed.). 2001. Water Use and Hydraulics in the Roman city, Colloquia and Conference Papers no. 3. Archaelogical Institute of America, Kendall/Hunt Publishing: Dubuque, IA; 131 pp.
Martinis B, Robba E. 1971. Note illustrative della Carta Geologica d'Italia alla scala 1:100.000, Foglio 202 "Taranto". Servizio Geologico d'Italia: Rome; 56.
Leucci G. 2004. Evaluation of 2-d resistivity and seismic refraction methods in a complex karstic area. *Geo Acta* **3**: 43–53.
Leucci G, Margiotta S, Negri S. 2004. Geological and geophysical investigations in karstic environment (Salice Salentino, Lecce, Italy). *Journal of Environmental and Engineering Geophysics* **9**: 25–34.
Leucci G, De Giorgi L. 2010. Microgravimetric and ground penetrating radar geophysical methods to map the shallow karstic cavities network in a coastal area (Marina di Capilungo, Lecce – Italy). *Exploration Geophysics* **41**: 178–188.
Loke MH, Barker RD. 1996. Rapid least-squares inversion of apparent resistivity pseudosections using a quasi-Newton method. *Geophysical Prospecting* **44**: 131–152.
Mays LW, Koutsoyiannis D, Angelakis AN. 2007. A brief history of urban water supply in the antiquity. *Water Science and Technology: Water Supply* **7**(1): 1–12.
Munjiza A. 2004. The Combined Finite-discrete Element Method. John Wiley & Sons: Chichester.
Nuzzo L, Leucci G, Negri S. 2004. Gpr survey in the karstic area near Nociglia (Lecce, Italy). In *Proceedings, Tenth International Conference on Ground Penetrating Radar*, 21–24 June, Delft, The Netherlands; 609–612.
Parise M. 2009. Distribution and characteristics of ancient underground aqueducts in Italy. In *Proceedings, International Water Association Specialty Conference, 2nd International Symposium on 'Water and wastewater technologies in ancient civilizations'*, Bari, 28–30 May.
Parise M. 2011. Managing water resources in the karst of southern Italy: an historical survey. In *Proceedings, H2Karst, 9th Conference on Limestone Hydrogeology*, Besançon, France, 1–3 September; 383–386.
Parise M, Gunn J (Eds). 2007. Natural and Anthropogenic Hazards in Karst Areas: Recognition, Analysis and Mitigation, special publication no. 279. Geological Society: London.
Parise M, Sammarco M. 2015. The historical use of water resources in karst. *Environmental Earth Sciences* **74**: 143–152. DOI:10.1007/s12665-014-3685-8.
Parise M, Federico A, Delle Rose M, Sammarco M. 2003. Karst terminology in Apulia (southern Italy). *Acta Carsologica* **32**(2): 65–82.
Parise M, Bixio R, Burri E, *et al.* 2009. The map of ancient underground aqueducts: a nation-wide project by the Italian Speleological Society. In *Proceedings, 15th International Congress of Speleology*, Kerrville, Texas, 19–26 July; volume 3, 2027–2032.
Parise M, Marangella A, Maranò P, Sammarco M, Sannicola G. 2013. Collecting, transporting and storing water in karst settings of southern Italy: some lessons learned from ancient hydraulic systems. *Water Science Technology: Water Supply* **13**(3): 674–682.
Raikes RL. 1966. Beidha prehistoric climate and water supply. In *Five Seasons at the Pre-pottery Neolithic Village of Beidha in Jordan*, Kirkbride D (ed.) *Palestine Exploration Quarterly* **98**: 68–72.
Sammarco M, Parise M, Martimucci V, Pepe P. 2010. The contribution of GPR analysis to knowledge of the cultural heritage in Apulia (southern Italy). In *Proceedings, XIII International Conference on Ground Penetrating Radar*, Lecce, Italy, 21–25 June; 70–76.
Sandmeier KJ. 2013. Reflexw 7.0 manual. Sandmeier Software: Karlsruhe.
Teuma EP. 2005. Qanat, saqqajja and roman aqueduct system at Rabat, Malta. In Proceedings, History Week 2003. Historical Society of Malta: Floriana; 43–56.
Trogu A, Ranieri G, Calcina S, Piroddi L. 2014. The ancient roman aqueduct of Karales (Cagliari, Sardinia, Italy): applicability of geophysics methods to finding the underground remains. *Archaeological Prospection* **21**(3): 157–168.
Yilmaz O. 1987. Seismic data processing. In Seismic Data Processing, Neitzel EB (ed). Society of Exploration Geophysicists: Tulsa, OK.
Zorzi L, Reina C. 1962. Idrogeologia della Provincia di Taranto. *Giornale del Genio Civile* **2**: 149–165.

DOI: 10.1002/arp